Input-output analysis of high-speed jet noise

By J. W. Nichols† AND M. R. Jovanović‡

We use input-output analysis to examine subsonic and supersonic turbulent jet noise. For a supersonic jet, the leading input-output mode closely resembles wavepackets resulting from the parabolized stability equations (PSE). For a subsonic jet, however, input-output analysis produces several sub-optimal modes with nearly the same gain as the leading input-output mode. The sub-optimal modes depend upon spatially extended input forcings and thus cannot be predicted by PSE. This may explain why PSE modes successfully predict far-field acoustics of supersonic jets but severely underpredict the farfield acoustics of subsonic jets.

1. Introduction

Analysis of laboratory measurements and large scale simulations have shown that instability wavepackets can be used to statistically model acoustic sources associated with subsonic jets (Suzuki & Colonius 2006). Furthermore, such wavepackets can be computed efficiently using the parabolized stability equations (PSE), and used for reduced-order models of the noise generation (Cheung *et al.* 2007; Gudmundsson & Colonius 2011). Although the PSE-computed wavepackets agree well with laboratory measurements of supersonic jets, larger discrepancies are encountered in the case of subsonic jets (Rodriguez *et al.* 2013).

Recently, high-fidelity large eddy simulations (LES) of ideally expanded isothermal and heated supersonic jets, corresponding to an experiment performed at UTRC, have been performed using the CharLES compressible flow solver (Brès *et al.* 2012). Using a hybrid FWH/LES approach, blind comparison showed that the simulation predicted far-field acoustic measurements. Comparison of this same data to PSE wavepackets computed about the mean flow of the simulations showed promising agreement for a range of frequencies, but at some frequencies, the agreement broke down. The agreement was worst for low frequencies (where the assumption of slowly-developing base flow implicit in PSE breaks down compared with the wavelength) and for heated jets.

Whereas linear wavepackets are able to predict both the near-field pressure fluctuations and the far-field acoustics in the case of supersonic jets (Sinha *et al.* 2014), acoustic prediction from near field wavepackets is less straightforward (Jordan & Colonius 2013). In subsonic jets, the peak of the near-field spectrum is not in the radiating range, so intermittency may play a dominant role. For subsonic jets, the amplitude acoustic field computed from non-intermittent wave packets tends to be significantly underpredicted. Although intermittency may arise from temporal nonlinear interaction between mid-frequency wavepackets and low-frequency modifications to the base flow about which they oscillate (Cavalieri *et al.* 2011), in this report we note that it may also arise from the spatial intermittency of the turbulence. In particular, we consider the behavior of small perturbations about a mean flow, driven by spatially extended stochastic forcing

† Department of Aerospace Engineering and Mechanics, University of Minnesota
‡ Department of Electrical and Computer Engineering, University of Minnesota

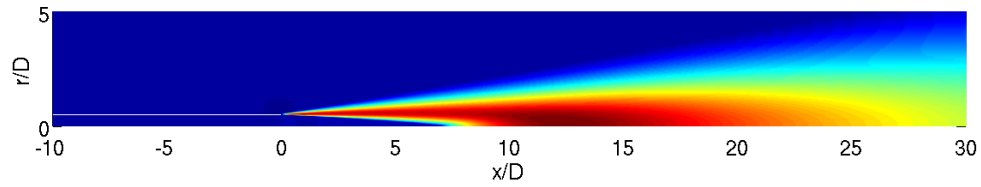

FIGURE 1. Contours of temperature for the $M_j = 1.5$ jet.

supplied by the turbulence. An input-output analysis (Jovanović & Bamieh 2005) is employed to identify the spatial structure of the forcing functions that optimally convert near-field aerodynamic fluctuations into far-field acoustic radiation for both a supersonic and a subsonic jet.

2. Methodology

2.1. *Base flows*

In order to begin analysis of small but coherent perturbations in the field of a statistically stationary turbulent jet, we adopt solutions to the Favre-averaged Navier-Stokes (FANS) equations as base flows about which to linearize. Mathematically, linearizing about the FANS equations is not strictly acceptable because coherent perturbation modes that we compute feedback through the Reynolds stresses to modify the base flow. While this is indeed the case for many flows controlled by instabilities, stability modes computed about time-averaged turbulent base flows for high-speed jets closely agree with embedded coherent motions measured in experiments (Gudmundsson & Colonius 2011; Cavalieri *et al.* 2013). This may be due to the fact that, while high-speed jets contain significant turbulent kinetic energy associated with aerodynamic fluctuations, the energy associated with coherent fluctuations responsible for acoustic radiation is much smaller. Furthermore, we show that the choice of input-output pairs allows us to focus more directly upon only those dynamics that directly produce far-field sound. This provides additional justification for our choice of base flows.

The FANS equations were computed using a modified $k - \epsilon$ turbulence model with coefficients recommended by Thies & Tam (1996) and validated for a range of compressible, turbulent round jets. To compare differences in noise generation between supersonic and supersonic jets, we specifically consider two isothermal high-speed jets, one with jet Mach number $M_j = 1.5$ and the other with $M_j = 0.9$. Here, the jet Mach number is defined by $M_j = u_j/c_j$ where u_j is the nozzle exit velocity and c_j is the speed of sound in the center of the jet. Both jets are isothermal meaning that the temperature inside the potential core of the jet matches that of the ambient fluid, although viscous heating causes the shear layers to become hot, as shown in Figure 1. In this case, the acoustic Mach number, defined as $M_a = u_j/c_\infty$ where c_∞ is the speed of sound in the ambient fluid, matches the jet Mach number exactly.

2.2. *Linearized governing equations*

To model the dynamics of small perturbations about our chosen base flows, we apply Goldstein's form of the linearized Euler equations as follows (Goldstein 2003). In an acoustic analogy, these equations would be balanced on the right hand side by the inhomogeneous nonlinear terms resulting from an exact rearrangement of the compressible Navier-Stokes equations. Because this particular form of the linearized Euler equations

takes into account propagation effects of refraction from both convection and temperature, Goldstein argues that the remaining acoustic source terms are simpler than other acoustic analogies found in the literature. Without the source terms, the homogeneous linearized Euler equations are

$$\bar{\rho}\frac{\bar{D}}{Dt}\frac{\rho'}{\bar{\rho}} + \frac{\partial}{\partial x_j}\bar{\rho}u_j' = 0, \tag{2.1}$$

$$\bar{\rho}\left(\frac{\bar{D}}{Dt}u_i' + u_j'\frac{\partial \tilde{v}_i}{\partial x_j}\right) + \frac{\partial}{\partial x_i}p_e' - \frac{\rho'}{\bar{\rho}}\frac{\partial \tilde{\tau}_{ij}}{\partial x_j} = 0, \tag{2.2}$$

$$\frac{1}{\gamma-1}\left(\frac{\bar{D}}{Dt}p_e' + \gamma p_e'\frac{\partial \tilde{v}_j}{\partial x_j} + \gamma\frac{\partial}{\partial x_j}\bar{p}u_j'\right) - u_i'\frac{\partial \tilde{\tau}_{ij}}{\partial x_j} = 0. \tag{2.3}$$

Here, $(\bar{\ })$ denotes a time-averaging, $(\tilde{\ })$ denotes a Favre-averaging, and $\bar{D}/Dt$ is the convective derivative with respect to the Favre averaged velocity. The time average density $\bar{\rho}$, pressure $\bar{p}$, and Favre averaged velocity $\tilde{v}_i$ are taken from the FANS base flow, as is the base flow total stress tensor $\tilde{\tau}_{ij}$. The perturbation state is then described by the quantities

$$\frac{\rho'}{\bar{\rho}}, \quad u_i' = \frac{\rho v_i''}{\bar{\rho}}, \quad p_e' = p' + \frac{(\gamma-1)}{2}\rho v''^2 + (\gamma-1)\tilde{H}_0,$$

which are density-like, velocity-like, and pressure-like perturbations, respectively. Here, $\rho' = \rho - \bar{\rho}$, $p' = p - \bar{p}$, and $v_i'' = v_i - \tilde{v}_i$.

The linearized Euler equations can be written abstractly as

$$\frac{\partial q}{\partial t} = Aq, \tag{2.4}$$

where $q = [\rho'/\bar{\rho},\, u_i',\, p_e']^T$ and the linear operator A depends on the base flow $\bar{\rho}$, $\bar{p}$, $\tilde{v}_i$, and $\tilde{\tau}_{ij}$. Although compact, this equation appeared in many 2014 CTR summer program presentations, including once in twenty-foot tall fonts.

3. Results and discussion

3.1. *Stability analysis*

At this point, we can consider the stability of this linearized system by using the following ansatz to search for wavelike modes that satisfy Eq. (2.4).

$$q(x, r, \theta, t) = \hat{q}(x, r)e^{im\theta - i\omega t}. \tag{3.1}$$

Here we assume azimuthal wavenumber $m = 0$. Substituting Eq. (3.1) into the linearized system Eq. (2.4) yields a two dimensional eigenvalue problem for the complex frequency $\omega = \omega_r + i\omega_i$:

$$-i\omega\hat{q} = A\hat{q}. \tag{3.2}$$

This eigenvalue problem can be solved numerically for the most significant eigenvalues using an iterative method such as the implicitly restarted Arnoldi method (IRAM) (Lehoucq *et al.* 1998). Figure 2(a) shows the spectrum of eigenvalues resulting from such a stability analysis applied to the $M_j = 1.5$ high speed jet. The nondimensional frequency associated with a mode is given by the Strouhal number $St_r = \omega_r D/(2\pi u_j)$, where D and u_j are the nozzle exit diameter and velocity, respectively. Similarly, $St_i = \omega_i D/(2\pi u_j)$ corresponds to a mode's temporal growth rate. The supersonic jet is globally stable, since

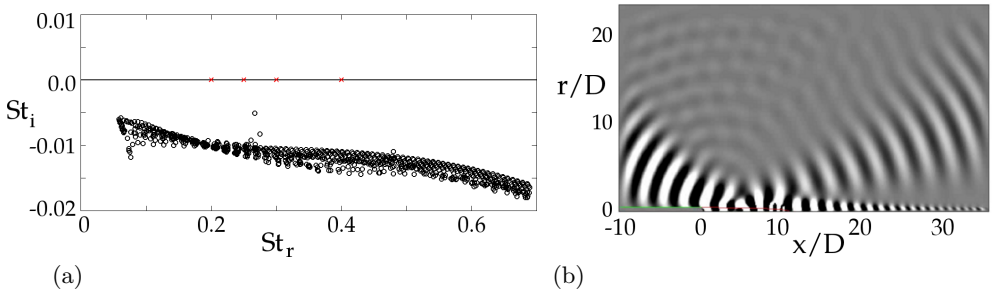

FIGURE 2. (a) The global eigenvalue spectrum for the $M_j = 1.5$ isothermal jet. (b) A stable, discrete global mode. Contours of the real part of perturbation pressure are shown.

all of the eigenvalues lie in the stable lower half plane. Because the computational domain is infinite in both the x and r directions, most of the eigenvalues are associated with a cloud completely covering a portion of the complex ω plane. These eigenvalues comprise a continuous spectrum and describe acoustic propagation away from the jet. In addition to the acoustic spectrum, there are also a few discrete modes that separate themselves from the rest of the spectrum. These modes arise from the finite width and length of the jet potential core.

A particular discrete mode is shown in Figure 2(b). Contours of the real part of the perturbation pressure show the clear growth and decay of an aerodynamic wavepacket along the axis of the jet. Connected to this wavepacket are two acoustic beams that propagate away from the jet in both the upstream and downstream directions. Counterintuitively, the amplitude of the upstream-propagating acoustic wave appears to grow along the beam propagation direction until reaching the boundary. Likewise, downstream-propagating acoustic waves do not appear to decrease as one might expect from radial spreading. To model the Sommerfeld radiation condition and avoid unphysical reflections, however, the computational domain is surrounded by numerical sponge layers at the upstream, downstream, and lateral boundaries. Once an acoustic beam reaches the sponge layer, its amplitude begins to decrease.

In the framework of global modes, the origin of this spatial growth can be understood by considering a simple model of the one-dimensional two-way wave equation surrounded by a sponge zone at both upstream and downstream boundaries. An initial disturbance will create left and right running waves that propagate with constant amplitude until reaching the sponge layers, after which they will damp. Therefore, this system is stable: no disturbances can remain in the system in the long-time limit. Since the wave equation is linear, we can easily compute eigenfunctions: an example is shown in Figure 3. Further, we consider the evolution of this mode according to $\hat{q}e^{-i\omega t}$ and plot q at several different intervals. Note that since the system is stable, $\omega_i < 0$ and the overall amplitude of the mode decays in time. However, the amplitude of an individual wavecrest is maintained as it propagates toward the boundary. In fact, the spatial growth of the mode is exactly ω_i/c, which preserves this property (Nichols & Lele 2011*a*).

Since stable global modes grow in space away from acoustic sources, they violate the Sommerfeld radiation condition. For this reason, they are usually discarded. We argue, however, the stable modes form a basis that describes propagation, and thus do indeed have meaning, as a group. Unfortunately, because of spatial growth, the basis provided by global modes for acoustic propagation is ill-conditioned. The total amount of growth contained in a mode is governed by both the amount of temporal damping $-\omega_i$ and

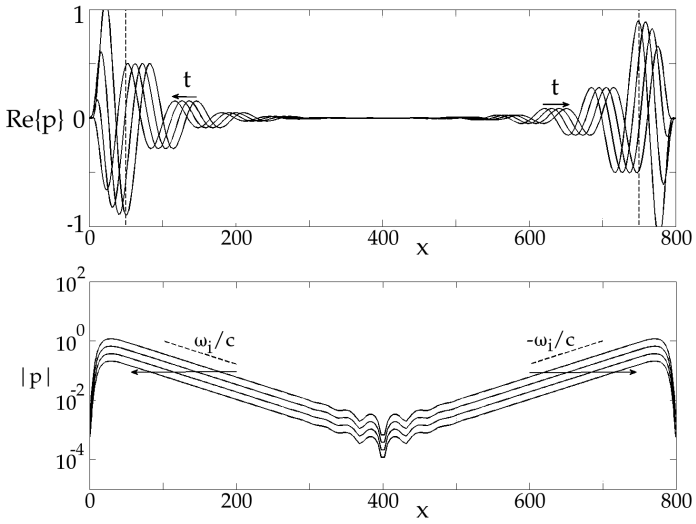

FIGURE 3. The temporal evolution of a global mode of the two-way wave equation. The vertical dashed lines at $x = 50$ and $x = 750$ in the top panel indicate the beginning of the sponge layers on both edges of the domain.

the size of the computational domain. As spatial growth increases, the energy of all of the modes becomes concentrated around the edges of the domain and at some point, a finite precision computer can no longer resolve the interior of the domain (Nichols & Lele 2011*b*; Garnaud *et al.* 2013*b*,*a*). Also, because all of the stable global modes more or less follow this pattern, they all lie in approximately the same direction in Hilbert space and thus are highly non-orthogonal. This is problematic for iterative methods such as IRAM, as the probability that random perturbations contain the right information to distinguish between two similar modes decreases as the method converges. For this reason, it took about a day using a single node of Certainty (24 cores) to compute the spectrum shown in Figure 2(a).

3.2. *Input-output analysis*

Global mode analysis is a powerful tool for systems dominated by unstable modes. Such systems behave as oscillators and support self-sustained oscillations. The high-speed jets we consider in this report are globally stable, meaning that all zero group velocity modes decay in time. They are, however, highly unstable to convective perturbations in the form of wavepackets (Jordan & Colonius 2013). In this way, these jets can be thought of as amplifiers, that depend on external perturbations as inputs. In this section, we therefore treat high-speed compressible jets as amplifiers, analyzing the sensitivity of the noise they output to external disturbances. In particular we consider our original linear system with applied forcing u

$$\dot{q} = Aq + Bu, \tag{3.3}$$

$$y = Cq, \tag{3.4}$$

with y being quantities of interest. For a given frequency ω, the transfer function from inputs $u = \hat{u}e^{zt}$ to outputs $y = \hat{y}e^{zt}$ is

$$H = C\left(zI - A\right)^{-1} B, \tag{3.5}$$

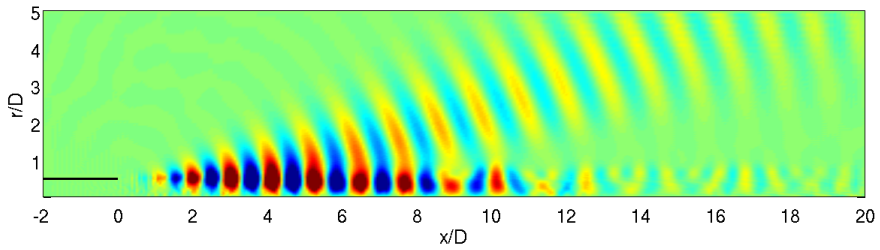

FIGURE 4. Contours of the real part of pressure-like perturbations displaying a wavepacket computed using input-output analysis. This mode corresponds to the output associated with the largest singular value using the pressure-norm to select inputs and outputs. The total compute time for this mode was less than one minute.

where $z = -i\omega$. Using singular value decomposition, H may be decomposed as

$$H = U\Sigma V^*, \tag{3.6}$$

where U and V are unitary matrices and Σ is a matrix of singular values. Here $(\ )^*$ denotes the complex-conjugate transpose. Rearranging,

$$HV = U\Sigma, \tag{3.7}$$

so that each column of V is an input vector that is mapped to the corresponding column of U through the transfer function H. The corresponding singular value represents the gain in amplitude from input to output. Singular values and vectors of H may be found through and eigenvalue decomposition of H^*H, or

$$H^*H = B^*(z^*I - A^*)^{-1}C^*C(zI - A)^{-1}B. \tag{3.8}$$

Here, A^* represents the discretized adjoint of our linear operator. Numerically, eigenvalues and vectors corresponding to the most significant singular values are solved simply through power iteration, or by applying an Arnoldi method (Nichols & Lele 2011*b*). Because H^*H is Hermitian, the resulting eigenvectors are orthogonal, and the Arnoldi method converges much more quickly. With this method the largest singular value and vector for a given frequency was computed in approximately one minute using one node of Certainty (24 cores).

The largest singular value σ_1 gives the maximum gain that can be achieved by a linear system. Figure 4 shows the corresponding output vector u_1 for the $\mathrm{M}_j = 1.5$ jet. Contours of the real part p_e are shown, and the field bears a striking similarity to wavepackets computed by PSE. The global framework places no restriction on the spatial structure of the base flow, however, and the response includes both upstream and downstream propagating waves. Furthermore, since responses to forcing at real frequencies are considered, the acoustic beam generated by the wavepacket does not suffer from spatial growth as did the global modes, and instead decays properly because of radial spreading.

Another advantage of input-output analysis is that the matrices B and C can be selected to capture inputs and outputs of interest (Jovanović & Bamieh 2005). For Figure 4, both B and C were chosen to select p_e from the state variable, so that the gain is measured with respect to the pressure-norm. The space of outputs can also be spatially separated from the space of allowed inputs. In Figure 5, we chose the inputs to be restricted to velocity-like perturbations u_e in the region $0 < r/D < 2$, whereas the

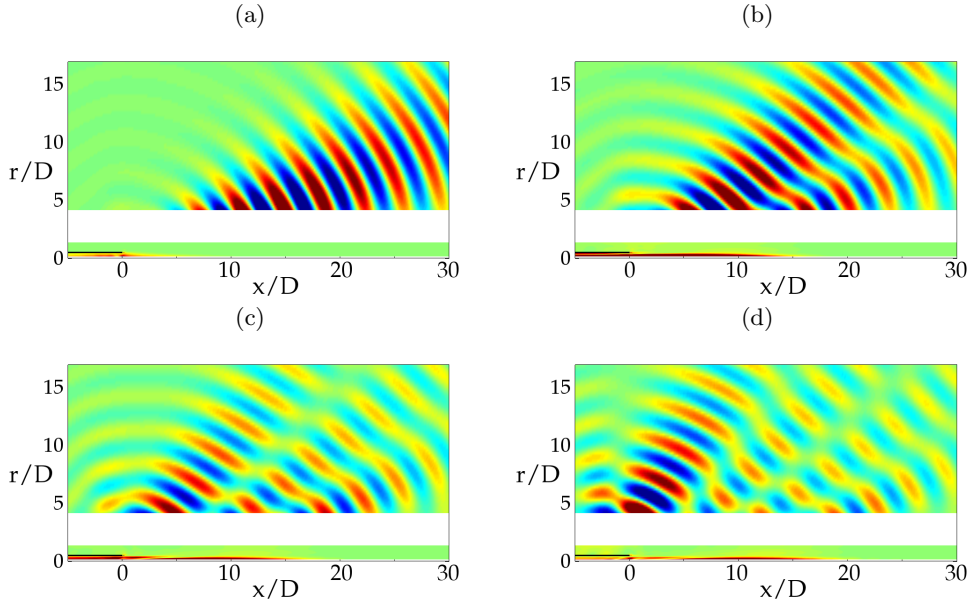

FIGURE 5. The four input-output modes with largest gain for the $M_j = 1.5$ isothermal jet. Contours of the the magnitude of the velocity-like perturbation are shown in the near-field of the jet. The acoustic output is visualized by contours of the real part of the pressure-like perturbation in the farfield.

outputs were restricted to pressure-like perturbations in the region $r/D > 5$. Physically, this choice was meant to model our interest in how velocity fluctuations created inside the jet lead to far-field pressure fluctations. Another interesting B might be one that injects Goldstein's acoustic source terms into the u_e and p_e equations.

Figure 5 shows the first four input-output modes for the supersonic jet. The magnitude of the input velocity-like fluctuations u_e is shown in the near field, and the real part of the output pressure-like fluctuations p_e are shown in the far field. In the first input-output mode, a single acoustic beam radiates from the jet. Note that for this case, the input is localized spatially around x/D, and upstream within the nozzle. This may give some additional support to the PSE approach in the case of supersonic jets as PSE begins with an initial perturbation upstream and marches downstream as it calculates the mode. For the second, third, and fourth modes, however, the input appears more extended within the jet, so PSE would have a difficult time capturing these modes.

The output of the suboptimal modes follows an interesting pattern. In the second mode, two acoustic beams appear that radiate at a slightly higher angle and a slighty lower angle with respect to the jet axis than the single beam present in the first mode. Likewise, the output of the third mode contains three acoustic beams oriented at angles higher, lower, and in between the beam angles of the second mode. This interleaving of beam angles appears to continue to the higher modes. Furthermore, in the suboptimal modes, the strongest acoustic beam appears to rotate increasingly toward the sideline direction as the mode number increases. This suggests that suboptimal modes may provide a convenient and coherent basis upon which to model sideline radiation.

This analysis was repeated for the $M_j = 0.9$ jet, with results shown in Figure 6. Compared with the supersonic jet, note that the input of the first mode is less spatially confined, although the output more or less forms a single acoustic beam. As the mode

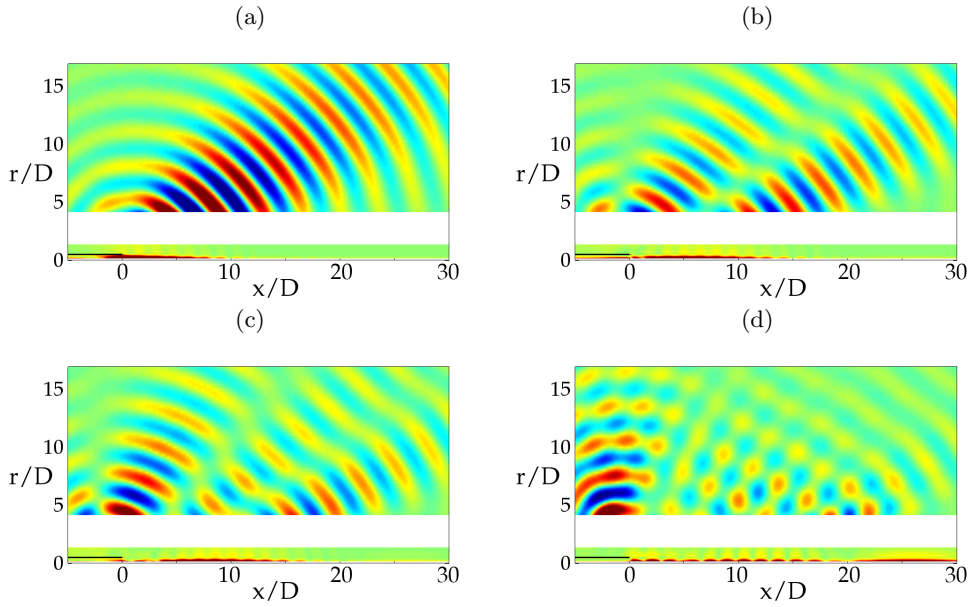

FIGURE 6. The four input-output modes with largest gain for the $M_j = 0.9$ isothermal jet. Contours of the the magnitude of the velocity-like perturbation are shown in the near-field of the jet. The acoustic output is visualized by contours of the real part of the pressure-like perturbation in the farfield.

number increases, the input shifts farther downstream inside the jet, and the output tends to rotate farther upstream.

Finally, Figure 7 compares the spectrum of singular values from the supersonic and subsonic calculations. In the supersonic case, the first singular value is about an order of magnitude larger than the next largest. Therefore, in this case, we expect most of the far-field noise to originate from the first input-output mode. Furthermore, because this mode contained a spatially localized input, we expect PSE to be successful in predicting the majority of the noise in a supersonic jet. The separation between the first and second modes is much less for the subsonic jet. In this case, the suboptimal modes should play a more signifcant role in determining the overall jet noise. Assuming each input-output mode is forced with unit energy the total energy in the outputs is $tr(H^*H)$ or the sum of squares of singular values. If we suppose that the first mode is captured by PSE, then compared with the energy contained in the first mode, by including the suboptimal modes the output energy would increase by only 0.3 dB in the supersonic case, but 6.7 dB in the subsonic case.

4. Conclusions

We have performed input-output analysis of small perturbations about FANS base flows for subsonic and supersonic isothermal high-speed jets. In the global framework, the input-output analysis directly considers the amplifying nature of the jets through a sensitivity analysis rather than relying upon stability modes. This is particularly relevant for the jet noise problem because only a small fraction of the fluctuations produced by the jet turbulence are converted into acoustic energy that radiates to the far-field. This is especially the case for subsonic jets. In this sense, the jet can be viewed as a filter

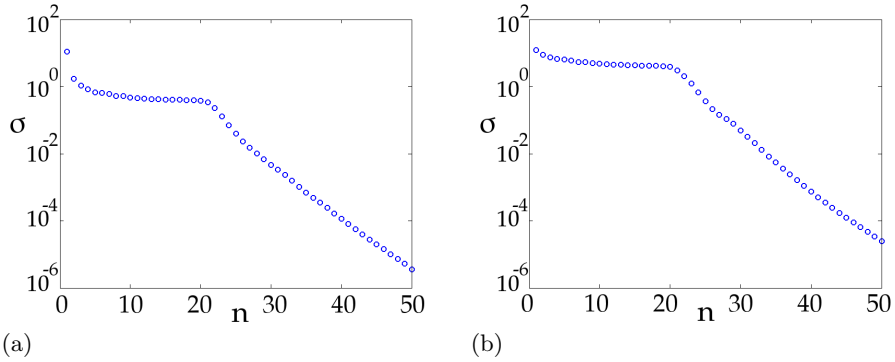

FIGURE 7. Singular values σ vs. mode number n for the (a) supersonic and (b) subsonic jets.

that extracts aeroacoustic energy from a large pool of aerodynamic energy. Furthermore, the input-output analysis allows us to restrict the spatial domain of inputs and outputs considered to study directly the transfer function between near field fluctuations and far-field noise.

For the supersonic jet, we recover a leading mode very similar to the convectively unstable wavepacket predicted by PSE. Compared with global mode calculations, this mode can be computed much more efficiently because the linear operator H^*H is Hermitian. It also incorporates upstream propagating waves, and can take into account abrupt changes in the base flow.

In addition to the leading order mode, the input-output analysis predicts a host of suboptimal modes that do not correspond to PSE modes, but nevertheless provide additional mechanisms by which aerodynamic near field fluctuations may be converted into far-field acoustic radiation. Some of the suboptimal modes are connected with sideline acoustic radiation. In the case of the subsonic jet, the gains of the suboptimal modes are nearly the same as the gain of the leading mode, which indicates that in this case including suboptimal modes may be important for predicting the correct overall farfield sound levels. On the other hand, the gain of the leading supersonic mode is nearly an order of magnitude greater than the next largest singular value, which indicates that PSE is capable of predicting most of the far-field noise in this case.

Acknowledgments

Computing resources have been provided by the Certainty cluster acquired under an NSF grant. The authors thank Prof. Taraneh Sayadi and Jinah Jeun whose careful comments on a preliminary version of this manuscript have helped improve it. JWN is grateful to Profs. Peter Jordan, Tim Colonius, Matthew Juniper, Peter Schmid, and Sanjiva Lele for many fruitful discussions about jet noise during the summer program and beyond.

REFERENCES

BRÈS, G., NICHOLS, J. W., LELE, S. K. & E., H. F. 2012 Towards best practices for jet noise predictions using unstructured large eddy simulations. *AIAA Paper 2012-2965*.

CAVALIERI, A. V. G., JORDAN, P., AGARWAL, P. & GERVAIS, Y. 2011 Jittering wavepacket models for subsonic jet noise. *J. Sound Vib.* **330**, 4474–4492.

Cavalieri, A. V. G., Rodriguez, D., Jordan, P., Colonius, T. & Gervais, Y. 2013 Wavepackets in the velocity field of turbulent jets. *J. Fluid Mech.* **730**, 559–592.

Cheung, L. C., Bodony, D. J. & Lele, S. K. 2007 Noise radiation predictions from jet instability waves using a hybrid nonlinear pse-acoustic analogy approach. In *Proceedings of the 13th AIAA/CEAS Aeroacoustics Conference (28th AIAA Aeroacoustics Conference)*.

Garnaud, X., Lesshafft, L., Schmid, P. J. & Huerre, P. 2013*a* Modal and transient dynamics of jet flows. *Phys. Fluids* **25**, 044103.

Garnaud, X., Lesshafft, L., Schmid, P. J. & Huerre, P. 2013*b* The preferred mode of incompressible jets: linear frequency response analysis. *J. Fluid Mech.* **716**, 189–202.

Goldstein, M. 2003 A generalized acoustic analogy. *J. Fluid Mech.* **488**, 315–333.

Gudmundsson, K. & Colonius, T. 2011 Instability wave models for near-field fluctuations of turbulent jets. *J. Fluid Mech.* **689**, 97–128.

Jordan, P. & Colonius, T. 2013 Wavepackets and turbulent jet noise. *Annual Rev. Fluid Mech.* **45**, 173–195.

Jovanović, M. R. & Bamieh, B. 2005 Componentwise energy amplification in channel flows. *J. Fluid Mech.* **534**, 145–183.

Lehoucq, R. B., Sorensen, D. C. & Yang, C. 1998 *ARPACK Users' Guide: Solution of Large-Scale Eigenvalue Problems with Implicitly Restarted Arnoldi Methods*. SIAM.

Nichols, J. W. & Lele, S. K. 2011*a* Global modes and transient response of a cold supersonic jet. *J. Fluid Mech.* **669**, 225–241.

Nichols, J. W. & Lele, S. K. 2011*b* Non-normal global modes of high-speed jets. *Int. J. Spray Comb. Dyn.* **3**, 285–302.

Rodriguez, D., Sinha, A., Bres, G. A. & Colonius, T. 2013 Inlet conditions for wave packet models in turbulent jets based on eigenmode decomposition of large eddy simulation data. *Phys. Fluids* **25**, 105107.

Sinha, A., Rodriguez, D., Bres, G. A. & Colonius, T. 2014 Wavepacket models for supersonic jet noise. *J. Fluid Mech.* **742**, 71–95.

Suzuki, T. & Colonius, T. 2006 Instability waves in a subsonic round jet detected using a near-field phased microphone array. *J. Fluid Mech.* **565**, 197–226.

Thies, A. T. & Tam, C. K. W. 1996 Computation of turbulent axisymmetric and nonaxisymmetric jet flows using the k-epsilon model. *AIAA J.* **34**, 309–316.